Comparing Elastomeric Behavior of Block and Random Ethylene–Octene Copolymers

H. P. Wang,[1] S. P. Chum,[2] A. Hiltner,[1] E. Baer[1]

[1]*Department of Macromolecular Science and Engineering, Center for Applied Polymer Research, Case Western Reserve University, Cleveland, OH 44106-7202*
[2]*Polyolefins and Elastomers R&D, The Dow Chemical Company, Freeport, Texas 77541*

Received 24 November 2008; accepted 19 January 2009
DOI 10.1002/app.30070
Published online 7 May 2009 in Wiley InterScience (www.interscience.wiley.com).

ABSTRACT: This work compared the elastomeric properties of two low-crystallinity ethylene–octene copolymers. One was a block copolymer with lamellar crystals and the other was a random copolymer with fringed micellar crystals. The comparison of the stress–strain behavior at 23°C revealed that the initial elastic modulus and the yield stress depended only on the crystallinity of the copolymer. When the temperature was raised above 23°C, melting of the fringed micellar crystals of the random copolymer caused a rapid decrease in the modulus. Some decrease in the modulus of the block copolymer over the same temperature range was attributed to the crystalline α-relaxation. Both polymers exhibited strain-hardening, ultimate fracture at high strains, and high recovery after fracture. However, in the block copolymer, the onset of strain-hardening and the ultimate fracture occurred at higher strains. The block copolymer also showed higher recovery from high strains. The initial stretching resulted in a permanent change in the stress–strain curve. It was suggested that following the onset of crystal slippage at the yield, the crystals underwent permanent structural changes through the course of the strain-hardening region. The transformation of the fringed micellar crystals occurred at lower strains than the transformation of the lamellar crystals. The extent of the structural transformation was described by the crosslink density and the strain-hardening coefficient extracted from elasticity theory. © 2009 Wiley Periodicals, Inc. J Appl Polym Sci 113: 3236–3244, 2009

Key words: ethylene–octene copolymers; olefin block copolymers; olefin elastomers

INTRODUCTION

Polyolefin-based thermoplastic elastomers (TPEs) have received considerable attention due to their chemical inertness, low density, and low cost compared with other TPEs.[1] Since olefin copolymers became commercially available in the 1960s,[2] a sizable effort has been expended to develop catalyst technology[3] and structure–property relationships for very low crystallinity olefin copolymers.[4–11] To obtain elastomeric properties of low modulus and high recovery from large deformations, the crystallinity is usually less than 20 wt %. The crystals act as reinforcements and as physical crosslinks to connect the rubbery, amorphous segments with high comonomer content. The crystallinity is provided by the ethylene or propylene sequences that are long enough to crystallize. In random ethylene–octene (EO) copolymers, the crystallizable ethylene sequences form fringed micellar crystals that act as the network junctions.[12] However, the statistical distribution of crystallizable chain lengths in the random copolymers results in a broad crystal size distribution and a low melting temperature, which limits their application at higher temperatures.[13,14]

The novel polyolefin chain shuttling catalyst technology developed by The Dow Chemical Company has enabled the synthesis of olefin multiblock copolymers in a continuous process.[15] The block copolymers of interest here consist of crystallizable EO blocks with very low comonomer content and high melting temperature, alternating with amorphous EO blocks with high comonomer content and low glass transition temperature. The multiblock architecture shows a distribution in block lengths and a distribution in the number of blocks per chain,[16] which differentiates it from anionically polymerized and hydrogenated olefin block copolymers. However, the crystallizable blocks are long enough to form chain-folded lamellar crystals with the orthorhombic unit cell and high melting temperature. Because of the unique block structure, the olefin block copolymers (OBCs) do not follow many of the traditional structure/property relationships established for random polyolefin elastomers.[17] The

Correspondence to: A. Hiltner (ahiltner@case.edu).
Contract grant sponsor: The Dow Chemical Company.

TABLE I
Characteristics of Block and Random Ethylene–Octene Copolymers

Polymer	Total octene (mol %)	M_w (kg/mol)	M_w/M_n	I_2[a] (g/10 min)	Density (g/cm^3)	T_m (°C)	ΔH_m[b] (J/g)	X_c[c] (wt %)	T_g[d] (°C)
OBC88	12.2	124	2.1	1.4	0.8795	118	49	17	−42
EO87	11.6	111	2.1	1.0	0.8724	061	38	13	−36

[a] Melt flow index.
[b] Heat of melting from the first-heating endotherm.
[c] Crystallinity from heat of melting.
[d] Glass transition temperature from dynamic mechanical thermal analysis tan δ.

block copolymers exhibit faster crystallization[18] and improved adhesion properties[19] compared with random copolymers.

It is expected that the lamellar crystallization habit of the block copolymers will impart elastomeric properties that are significantly different from those of the random copolymers with fringed micellar crystals. In the present study, a side-by-side comparison was made between the elastomeric response of a block and a random EO copolymer that are closely matched in comonomer content, density, and crystallinity.

MATERIALS AND METHODS

The block EO copolymer was supplied by The Dow Chemical Company (Freeport, TX), together with information on octene content, molecular weight, and molecular weight distribution as given in Table I. The detailed description of this block copolymer, including block length and block composition, can be found in a previous publication.[17] The weight percent of crystallizable hard block in this block copolymer was calculated to be 27% from the weight percent total octene and the weight percent octene in the hard/soft blocks. The commercial random EO copolymer with similar density as the block copolymer was used in this study for comparison. It was synthesized by the Dow's INSITE™ technology.[20] The block copolymer and the random copolymer were designated as OBC88 and EO87, respectively, with the number indicating its density (Table I). Both copolymers have approximately the same molecular weight, molecular weight distribution, and melt index (I_2, measured at 190°C at load of 2.16 kg). They were provided in the pellet form.

Plaques with the thickness of about 0.5 mm were compression-molded from the pellets at 190°C between Mylar® sheets and cooled to ambient temperature at ~ 15°C/min in the press. The compression-molded plaques were subsequently stored at ambient temperature for 7–12 days before measuring the physical and mechanical properties.

Density of the compression-molded plaques was measured using an isopropanol–water gradient column calibrated by glass beads. Thermal analysis was carried out with a Perkin Elmer (Boston, MA) Series 7 differential scanning calorimeter (DSC). Scans were taken between −50 and 190°C with a heating/cooling rate of 10°C/min. Weight percent crystallinity was calculated from the heat of melting in the first heating thermogram and was based on the heat of fusion of 290 J/g for perfect crystals.[21] Dynamic mechanical thermal analysis was carried out with a Polymer Laboratories (Amherst, MA) Dynamic Mechanical Thermal Analyzer. Specimens were tested in dynamic tension at less than 0.2% strain at 1 Hz from −80°C to 10°C below the melting temperature.

Microtensile specimens were cut from the compression-molded plaques according to ASTM D 1708. The tensile stress–strain behavior was measured with an MTS (Eden Prairie, MN) Alliance RT30 with the crosshead speed of 111.5 mm/min (500%/min based on the specimen gauge length). The engineering stress and strain were defined conventionally. In the hysteresis study, the specimens were cyclically loaded and unloaded in uniaxial tension at a crosshead speed 22.3 mm/min (100%/min based on the initial specimen gauge length). The hysteresis experiment was performed at various strains from 100 to 800%.

RESULTS AND DISCUSSION

Thermal behavior

The melting behavior of the block EO copolymer was characterized by a much higher melting temperature compared with the random EO copolymer with about the same density and comonomer content. The melting thermograms of OBC88 and EO87 are compared in Figure 1. Due to the long crystallizable ethylene sequence, the block copolymer showed a sharp melting peak, with the peak melting temperature at 118°C. In contrast, the melting range of the random copolymer with comparable density was located at a much lower temperature and was very broad, beginning at about ambient temperature and ending near 80°C. The ambient temperature aging

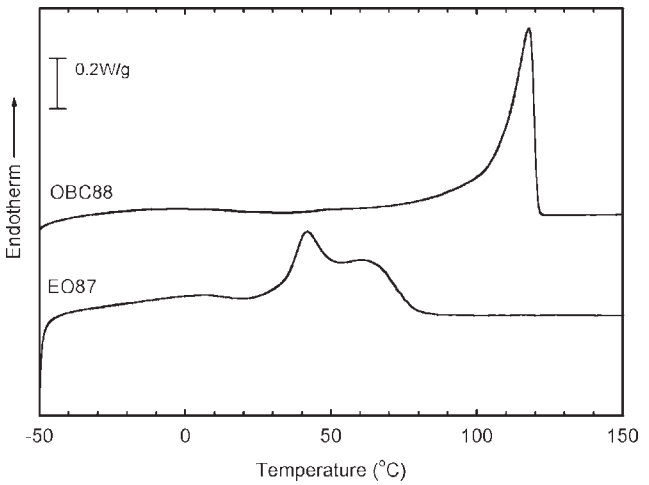

Figure 1 Comparison of the melting behavior of OBC88 and EO87. Specimens were aged 7–12 days after compression-molding. The first heating thermograms are shown here with the heating rate of 10°C/min.

peak in the random EO copolymer was found at 42°C. The low melting temperature and broad melting range of random EO copolymers were attributed to the fringed-micellar or bundle-like crystals with a broad size distribution that result from the statistical distribution of crystallizable chain lengths.[13,14] In contrast, the long ethylene sequences of the hard blocks in the block copolymers could crystallize as larger lamellar crystals with fewer defects and therefore much higher melting temperature.[22,23]

The temperature dependence of the dynamic mechanical relaxation behavior of both copolymers is compared in Figure 2 as the storage modulus (E'), the loss modulus (E''), and the loss tangent (tan δ). For OBC88, two primary relaxations were observed in the temperature range examined. The relaxation at high temperature, about 90°C in the tan δ curve, was identified as the α-relaxation of the hard segment crystalline phase. The low temperature β-relaxation is usually identified as the glass transition of the amorphous phase of ethylene copolymers.[24–26] Therefore, the β-relaxation peak temperature in the tan δ curve was taken as the glass transition temperature, T_g. For OBC88, the β-relaxation essentially reflected the glass transition of the soft segment, which comprised most of the amorphous phase. For EO87, only the β-relaxation was observed. The T_g of EO87 was slightly higher than that of OBC88 (Table I) because poorer crystal phase separation in the random copolymer resulted in an amorphous phase with lower octene content.

Stress–strain behavior

The uniaxial engineering stress–strain behaviors of the block and random EO copolymers at 23°C are compared in Figure 3(a). In both cases, the deformation was macroscopically uniform with large instantaneous strain recovery after fracture at high strains. The slightly higher modulus and yield stress of the block copolymer were attributed to the slightly higher crystallinity (Table II). The most striking differences in the stress–strain curves occurred at high strains where the onset of strain-hardening was seen at lower strains in EO87 than in OBC88. Because the engineering fracture stresses were about the same, the ultimate fracture strain of EO87 was less than that of OBC88 (Table II). The higher fracture strain

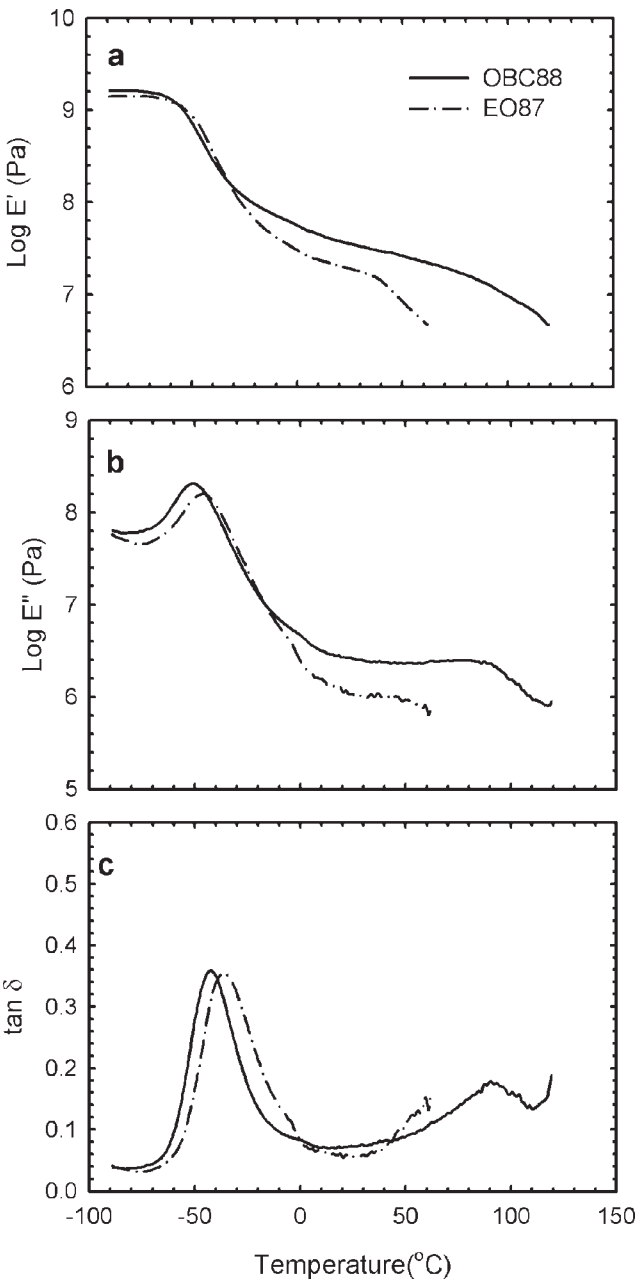

Figure 2 Comparison of the dynamic mechanical relaxation behavior of OBC88 and EO87 presented as (a) log E', (b) log E'', and (c) tan δ.

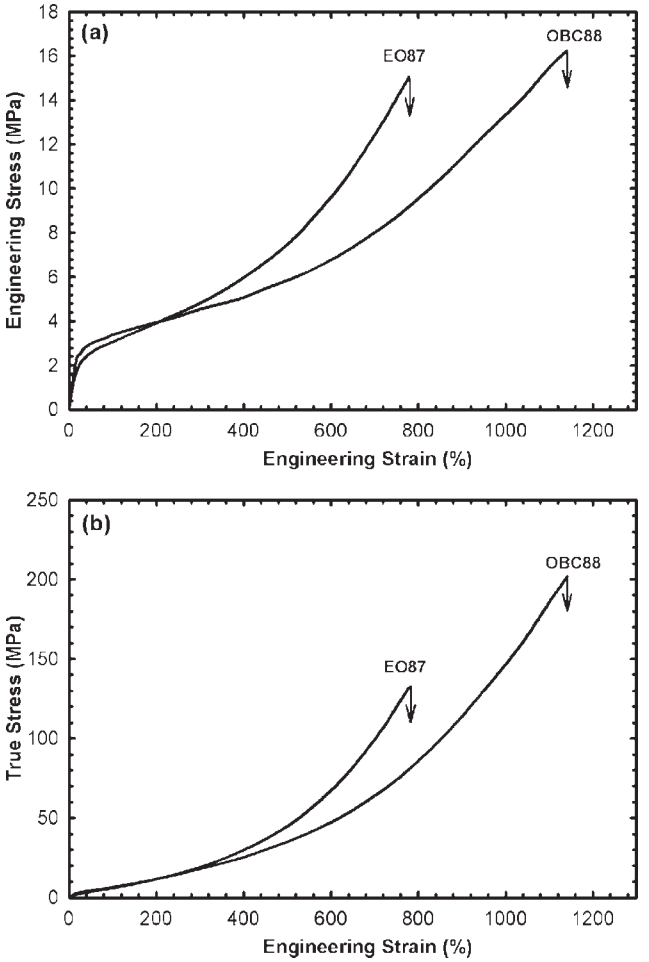

Figure 3 (a) Engineering stress–strain curves of OBC88 and EO87 copolymers at 23°C and a strain rate of 500%/min and (b) true stress–strain curves.

of OBC88, with similar engineering fracture stress as EO87, resulted in a higher toughness defined as the work expended to break the copolymer.

Considering that both the copolymers had similar molecular weights (M_w 110–125 kg/mol) and molecular weight distributions ($M_w/M_n \sim 2$), the difference in stress–strain behavior was attributed to differences in the deformation mechanism. It is imagined that initially, only the amorphous rubbery chains are stretched and the crystals serve as junctions and fillers. The modulus taken from the initial linear region of the stress–strain curve depends on the total crystallinity (filler effect). Thus it is not surprising that block and random copolymers with similar crystallinity also exhibit similar moduli. At higher strains, strain-hardening is associated with destruction of the crystals and reorganization as a highly oriented structure. The stress–strain curve indicates that the transformation of the bundle-like fringed micellar crystals in EO87 occurs at lower strains than the transformation of the lamellar crystals in OBC88.

The difference in stress–strain behavior is shown in terms of the true stress in Figure 3(b), where the true stress for uniform deformation σ_T is taken as the ratio of the load F on the specimen to the instantaneous minimum cross-sectional area A supporting that load

$$\sigma_T = \frac{F}{A} = \sigma\lambda = \sigma(1+\varepsilon) \quad (1)$$

where σ, λ, and ε are the engineering stress, extension ratio, and engineering strain, respectively. The true fracture stress of OBC88 is much higher than that of EO87, 200 MPa compared with 130 MPa, shown in Figure 3(b). Because the two copolymers have almost the same crystallinity, comonomer content, molecular weight, and molecular weight distribution, this dramatic difference is attributed to the difference in the oriented structure produced by drawing. From the practical point of view, such as in elastic fibers, the highly oriented structure of the block copolymer may have better mechanical strength than that of the random copolymer.

The effect of temperature on the tensile modulus is compared in Figure 4. The 30% secant modulus of OBC88 dropped to about half, from 8.6 MPa at 23°C to 4.4 MPa at 70°C. Over the same temperature range, the decrease in 30% secant modulus of EO87 was more substantial, from 6.6 MPa at 23°C to 1.0 MPa at 70°C. The larger decrease in the random copolymer was attributed to gradual melting of the fringed micellar crystals in this temperature range.[12] In contrast, no significant melting of the block copolymer occurred in this temperature range (Fig. 1). Rather, the decrease in modulus was identified with the gradual onset of the α-relaxation of the crystalline phase (Fig. 2). The α-relaxation is usually attributed to chain translation along the crystal axis and is thought to be responsible for the deterioration in

TABLE II
Parameters Describing the Elastomeric Stress–Strain Behavior of Block and Random Copolymers

Polymer	E[a] (MPa)	σ_y (MPa)	σ_f (MPa)	ε_f (%)	N_skT (MPa)	N_ekT (MPa)	α
OBC88	18 ± 1	2.9 ± 0.2	17 ± 3	1096 ± 66	14.9	0.63	0.042
EO87	13 ± 1	2.3 ± 0.2	15 ± 1	748 ± 29	12.2	0.69	0.064

[a] 5% secant modulus.

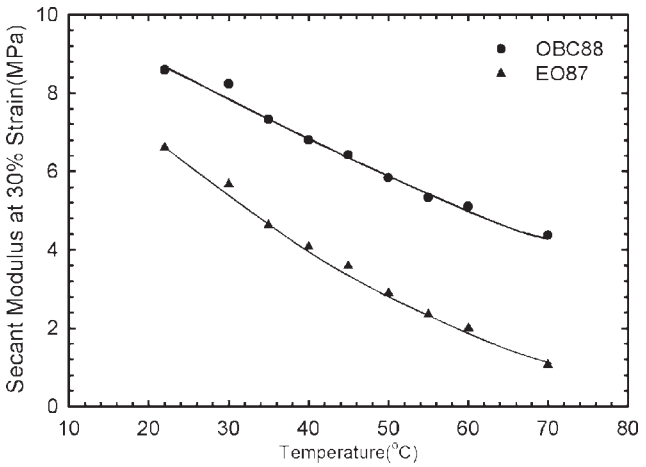

Figure 4 Temperature dependence of the secant modulus at 30% strain for OBC88 and EO87.

mechanical performance of crystalline polymers below the melting temperature.[24,25,27] The drop in the tensile modulus taken from the stress–strain curves corresponded with the drop in E' (Fig. 2) over the same temperature range.

Elastic strain recovery

The effect of repeated cyclic loading on the elastomeric behavior of block and random copolymers is shown in Figure 5. In these examples, the specimens were continuously cycled 10 times to 300% strain, based on the initial gauge length. For both block and random copolymers, a considerable change in the stress response occurred between the 1st cycle and the 2nd cycles. On the subsequent cycles there were small but consistent decreases in the stress response. The specimens exhibited a certain amount of unrecovered strain or "strain set" after the 1st cycle, with only a very small increase in the "strain set" on each subsequent cycle. It appeared that a significant and permanent structural change occurred during the 1st cycle that resulted in a "conditioned" material with better elastomeric recovery.[11,28] After the 1st cycle, the structural changes during subsequent cycles were rather insignificant, as indicated by the almost overlapping stress–strain curves. The major difference between the cyclic deformation behavior of the block and random copolymers was in the amount of "strain set" created in the 1st cycle. As indicated by the arrows in Figure 5, the "strain set" from 300% strain was about 75% in OBC88 compared with about 120% in EO87.

In other experiments, the copolymers were cycled to strains between 100 and 800%. To compare the effect of the imposed strain on the amount of recovery, a strain recovery parameter was defined as follows:

$$\text{Strain Recovery (\%)} = \frac{\varepsilon_{app} - \varepsilon_{rec}}{\varepsilon_{app}} \times 100 \qquad (2)$$

where ε_{app} is the applied strain and ε_{rec} is the unrecovered strain after the 1st cycle. The strain recovery at 23°C is plotted as a function of the applied strain in Figure 6(a). The dependence of strain recovery on the applied strain was somewhat different for OBC88 and EO87. The strain recovery decreased gradually with increasing applied strain for OBC88, whereas for EO87 the strain recovery decreased rapidly at lower applied strains and then leveled off at higher applied strains. As a consequence, for applied strains between 200 and 500%, OBC88 exhibited substantially higher recovery than EO87. For example, recovery from 200% strain was about 80% for OBC88 and only about 68% for EO87. This suggests that the largest changes in the crystalline structure

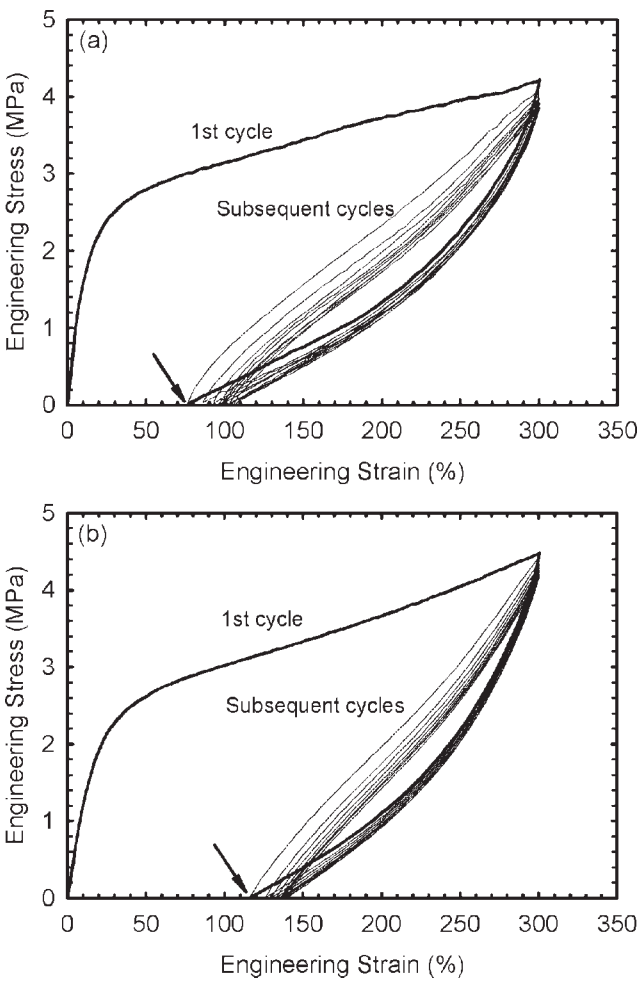

Figure 5 Comparison of the first loading and unloading cycles and the nine subsequent cycles to a strain of 300% for (a) OBC88 and (b) EO87. The engineering stress and strain were based on the initial specimen dimensions. The strain rate was 100%/min, based on the initial gauge length.

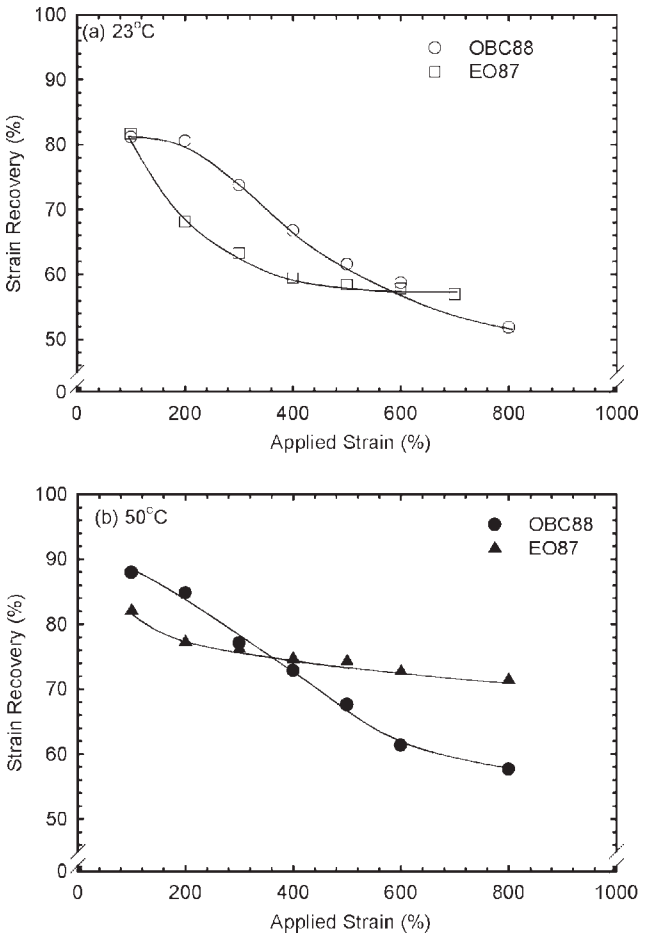

Figure 6 Comparison of the strain recovery from the first cycle for OBC88 and EO87 as a function of applied strain at (a) 23°C and (b) 50°C. Lines are drawn as guides.

of EO87 occurred at lower strains, whereas the structural changes in OBC88 occurred more gradually as the strain increased.

The strain recovery was also measured in hysteresis experiments performed at 50°C, as shown in Figure 6(b). The dependence of strain recovery on applied strain for OBC88 was about the same at 50°C and at 23°C. The decreasing trend in strain recovery with increasing applied strain at 50°C almost paralleled the trend at 23°C. However, for EO87 the strain recovery at 50°C was substantially higher than that at 23°C and the dependence on the applied strain was smaller. The difference between OBC88 and EO87 was attributed to the temperature-dependence of the crystallinity. Whereas the crystallinity of OBC88 did not change significantly over the temperature range from 23°C to 50°C, the crystallinity of EO87 dropped from 13 wt % at 23°C to 6 wt % at 50°C according to the DSC thermogram (Fig. 1). An increase in the elastic amorphous fraction resulted in higher strain recovery. Indeed, a random EO copolymer with lower crystallinity than EO87 showed higher strain recovery when compared at the same temperature.[29]

Sliplink model of elastomeric structure

The mechanical behavior of the block and random copolymers with low crystallinity complied with the concept of an elastomeric network with crystals serving as multifunctional junctions. However, morphologically the fringed micellar crystals of the random copolymer contrasted with the lamellar crystals of the block copolymer. The impact of this structural difference was probed by testing the experimental data against structural models of elasticity. A previous study demonstrated that the stress–strain curve of elastomeric random copolymers is well-described by the sliplink model, in which the lateral attachment and detachment of crystallizable chain segments at the crystal edges provide the sliding topological constraint attributed to sliplinks and the crosslinks represent permanent junctions, possibly created by chain entanglements that tighten into rigid knots upon stretching.[12] It was of interest to test the sliplink model against the stress–strain curve of the block copolymer and to compare the extracted parameters for block and random copolymers for insight into the role of the different crystalline structures.

Based on reptation concepts, the sliplink theory treats the network junctions as two types, sliplinks and crosslinks.[30,31] Sliplinks are mobile network junctions that restrict chain mobility until a sufficient force is applied, whereas crosslinks behave as permanent network junctions. In uniaxial extension, the total stress (σ) can be written as the sum of the contribution from sliplinks (σ_s) and crosslinks (σ_c):

$$\sigma = \sigma_s + \sigma_c \tag{3}$$

with

$$\sigma_s = N_s kT \left\{ \frac{(1+\eta)(1-\alpha^2)\alpha^2\left(\lambda-\frac{1}{\lambda^2}\right)}{\left[1-\alpha^2\left(\lambda^2+\frac{2}{\lambda}\right)\right]^2}\left(\frac{\lambda^2}{1+\eta\lambda^2}+\frac{2}{\lambda+\eta}\right) + \frac{(1-\alpha^2)(1+\eta)}{1-\alpha^2\left(\lambda^2+\frac{2}{\lambda}\right)}\left[\frac{\lambda}{(1+\eta\lambda^2)^2}-\frac{1}{(\lambda+\eta)^2}\right] + \frac{\eta\left(\lambda-\frac{1}{\lambda^2}\right)\lambda}{(1+\eta\lambda^2)(\lambda+\eta)}-\frac{\left(\lambda-\frac{1}{\lambda^2}\right)\alpha^2}{1-\alpha^2\left(\lambda^2+\frac{2}{\lambda}\right)}\right\} \tag{4}$$

and

$$\sigma_c = N_c kT\left(\lambda-\frac{1}{\lambda^2}\right)\left\{\frac{(1-\alpha^2)}{\left[1-\alpha^2\left(\lambda^2+\frac{2}{\lambda}\right)\right]^2}-\frac{\alpha^2}{1-\alpha^2\left(\lambda^2+\frac{2}{\lambda}\right)}\right\} \tag{5}$$

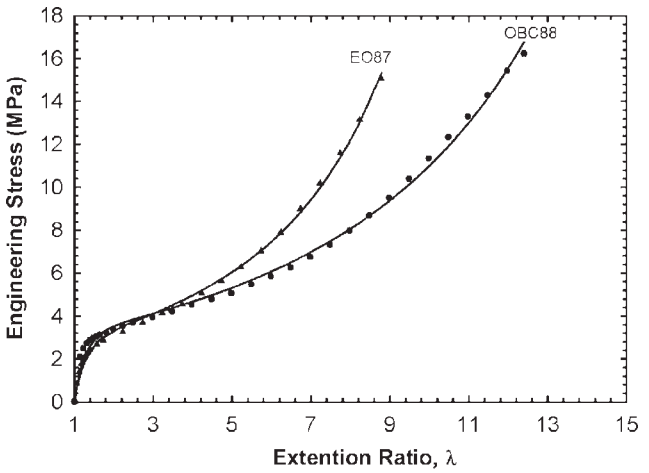

Figure 7 Comparison of stress–strain curves at 23°C calculated from sliplink theory (solid lines) with experimental results (data points).

where k is the Boltzman constant, T is the temperature in K, and λ is the draw ratio. The four material parameters operating in the equations are the density of crosslinked chains N_c, the density of sliplinks N_s, the slippage parameter η, and the inextensibility parameter α. Slippage allows for the decreasing modulus at low strains, and the parameter α describes the stress upswing at high strains. The data fit was carried out with η held constant at 1.1, the value reported for crosslinked polyethylene filaments stretched in the melt state.[32] A three-parameter, least-squares fit was performed to obtain N_s, N_c, and α for OBC88 and EO87. Good fits were obtained over the entire stress–strain curve (Fig. 7). The fitting parameters with $\eta = 1.1$ are listed in Table II.

The separate contributions of crosslinks and sliplinks to the total stress–strain curve are presented in Figure 8. For both copolymers the stress response at low strains ($\lambda < 2$) was governed primarily by the sliplink contribution. With increasing strain, the onset of slippage caused a rapid decrease in the initial high modulus. This produced a yield-like plateau before $\lambda = 2$. The sliplink density, which primarily determined the initial modulus and the plateau stress, was previously shown to correlate with the amount of crystallinity.[12] The slightly higher sliplink density of OBC88 compared with EO87 probably reflected the slightly higher crystallinity of OBC88 rather than an intrinsic effect of the different crystalline morphologies. It appeared that the initial modulus and yield-like plateau stress depended on crystallinity in the same way for block and random copolymers.

The crosslink contribution primarily determined the slope of the stress response at intermediate strains, whereas the inextensibility parameter determined how rapidly the stress increased in the strain-hardening region. A substantially higher value of α for EO87 described the onset of strain-hardening at a lower strain, which was the most striking difference in the stress–strain behavior of EO87 than in OBC88. The good fit of the stress–strain curve of the block copolymer to the sliplink model indicated that crystalline slippage also occurred in the lamellar crystals during stretching. However, the lower value of α of block copolymers demonstrated that the long, rubbery soft blocks were more easily stretched to higher strains than the much shorter amorphous blocks produced by the statistical comonomer distribution of random copolymers.

The initial stretching resulted in a permanent change in the stress–strain curve. It appeared that following the onset of crystal slippage at the yield, the crystals underwent permanent structural changes through the course of the strain-hardening region. The crystalline deformation is incorporated in the N_s term. The structural changes appear to be irreversible (Fig. 5), so the sliplink contribution may be absent from the 2nd and subsequent stress–strain curves. The strain on the 1st cycle was varied from 400 to 600%, and the subsequent loading curves for the 2nd cycle are shown in Figure 9. The stress and

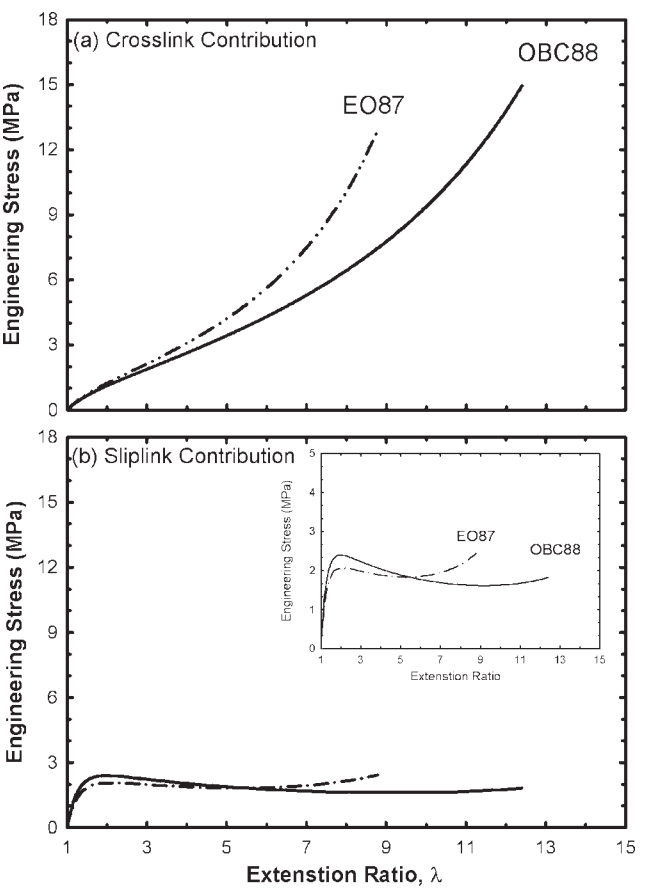

Figure 8 Separate contributions of (a) crosslinks and (b) sliplinks to the stress–strain curve.

strain were based on the sample dimensions at the end of the 1st cycle. It was found that if the applied strain on the 1st cycle was at least 400%, the subsequent stretching resulted in a stress–strain curve without the knee, which suggested the disappearance of sliplinks. The stress–strain data were tested against the two-parameter formulation in Eq. (5), which considers only crosslinks and inextensibility and is equivalent to the classical rubber theory. Eq. (5) did not describe the 2nd cycle curve if the strain on the 1st cycle was less than 400%, presumably because the crystalline structure was only partially transformed. However, if the strain on the 1st cycle was 400% or more, the fit was very good (Fig. 9). The values of N_c and α that gave the best fit are listed in Table III. Both N_c and α were substantially higher on the 2nd loading than in the 1st loading, indicating that the structural changes during the 1st loading produced a much stiffer structure. For OBC88, both N_c and α gradually increased as the strain on the 1st cycle increased, indicating continuing structural transformation through the strain-hardening region of the 1st cycle. The parameters were consistently higher for EO87 because strain-hardening and the associated structural changes occurred at lower strains on the 1st cycle. Indeed, the parameters for EO87 appeared to reach constant values at 500% 1st cycle strain, possibly indicating that the structural transformation was complete.

TABLE III
Model Parameters for the Second Cycle Stress–Strain Response of Block and Random Copolymers

Polymer	First cycle strain (%)	N_ckT (MPa)	α
OBC88	400	2.9	0.22
	500	3.2	0.27
	600	3.7	0.31
EO87	400	3.7	0.30
	500	4.0	0.34
	600	3.9	0.35

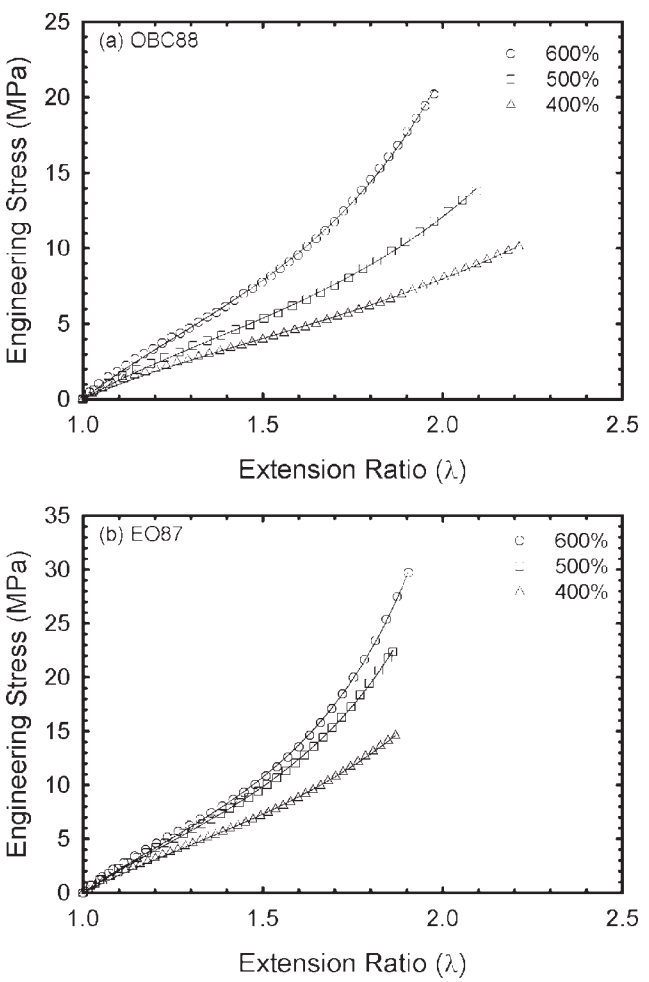

Figure 9 Fit of eq. (5) with the second cycle loading curve of (a) OBC88 and (b) EO87. Open points are experimental results and solid lines are the fit. Various applied strains in the first cycle are as labeled.

CONCLUSIONS

This work compared the elastomeric properties of a random EO copolymer and a block EO copolymer with similar densities. In these elastomers, the crystals act as reinforcements and as physical crosslinks to connect the rubbery, amorphous segments. It was anticipated that the lamellar crystallization habit of the block copolymer would result in elastomeric properties significantly different from those of the random copolymer with fringed micellar crystals. The comparison of the stress–strain behavior at 23°C revealed that the initial elastic modulus and the yield stress depended only on the crystallinity of the copolymer. It followed that the lower melting temperature of the fringed micellar crystals of the random copolymer caused a more rapid decrease in the modulus as the temperature was raised above 23°C. Some decrease in the modulus of the block copolymer over the same temperature range was attributed to the crystalline α-relaxation. Both polymers exhibited strain-hardening, ultimate fracture at high strains, and high recovery after fracture. However, in the block copolymer, the onset of strain-hardening occurred at a higher strain and the ultimate fracture strain was higher. The block copolymer also showed higher recovery from high strains.

The initial stretching resulted in a permanent change in the stress–strain curve. It was suggested that following the onset of crystal slippage at the yield, the crystals underwent permanent structural changes through the course of the strain-hardening region. The stress–strain curve indicated that the transformation of the bundle-like fringed micellar crystals in the random copolymer occurred at lower

strains than the transformation of the lamellar crystals in the block copolymer. This may have been because the long, rubbery, soft blocks were more easily stretched to high strains than the much shorter amorphous blocks produced by the statistical comonomer distribution of random copolymers. The extent of the structural transformation was described by the crosslink density and the strain-hardening coefficient extracted from elasticity theory. Considering the differences in crystallization habit of the random and the block copolymers, it seems likely that the transformation during stretching led to different oriented, crystalline morphologies.

The authors thank The Dow Chemical Company for their technical support.

References

1. Kresge, E. N. In Thermoplastic Elastomers, 3rd ed.; Holden, G.; Kricheldorf, H. R.; Quirk, R. P., Eds.; Hanser Publishers: Munich, 2004; Chapter 5, p 93.
2. Baldwin, F. P.; VerStrate, G. Rubber Chem Technol 1972, 45, 790.
3. Ostoja Starzewski, A.; Steinhauser, N.; Xin, B. S. Macromolecules 2008, 41, 4095.
4. Ver Strate, G. W.; Wilchinsky, Z. W. J Polym Sci Part A-2: Polym Phys 1971, 9, 127.
5. Androsch, R.; Stribeck, N.; Lupke, T.; Funari, S. S. J Polym Sci Part B: Polym Phys 2002, 40, 1919.
6. Wright, K. J.; Lesser, A. J. Macromolecules 2001, 34, 3626.
7. Liu, L.-Z.; Hsiao, B. S.; Fu, B. X.; Ran, S.; Toki, S.; Chu, B.; Tsou, A. H.; Agarwal, P. K. Macromolecules 2003, 36, 1920.
8. De Rosa, C.; Auriemma, F. Adv Mater 2005, 17, 1503.
9. Liu, L.-Z.; Hsiao, B. S.; Ran, S.; Fu, B. X.; Toki, S.; Zuo, F.; Tsou, A. H.; Chu, B. Polymer 2006, 47, 2884.
10. Toki, S.; Sics, I.; Burger, C.; Fang, D. F.; Liu, L. Z.; Hsiao, B. S.; Datta, S.; Tsou, A. H. Macromolecules 2006, 39, 3588.
11. Poon, B. C.; Dias, P.; Ansems, P.; Chum, S. P.; Hiltner, A.; Baer, E. J Appl Polym Sci 2007, 104, 489.
12. Bensason, S.; Stepanov, E. V.; Chum, S.; Hiltner, A.; Baer, E. Macromolecules 1997, 30, 2436.
13. Minick, J.; Moet, A.; Hiltner, A.; Baer, E.; Chum, S. P. J Appl Polym Sci 1995, 58, 1371.
14. Alizadeh, A.; Richardson, L.; Xu, J.; McCartney, S.; Marand, H.; Cheung, Y. W.; Chum, S. Macromolecules 1999, 32, 6221.
15. Arriola, D. J.; Carnahan, E. M.; Hustad, P. D.; Kuhlman, R. L.; Wenzel, T. T. Science 2006, 312, 714.
16. Shan, C. L. P.; Hazlitt, L. G. Macromol Symp 2007, 257, 80.
17. Wang, H.; Khariwala, D. U.; Cheung, W.; Chum, S. P.; Hiltner, A.; Baer, E. Macromolecules 2007, 40, 2852.
18. Khariwala, D. U.; Taha, A.; Chum, S. P.; Hiltner, A.; Baer, E. Polymer 2008, 49, 1365.
19. Dias, P.; Lin, Y. J.; Poon, B.; Chen, H. Y.; Hiltner, A.; Baer, E. Polymer 2008, 49, 2937.
20. Dow Plastics. ENGAGE polyolefin elastomers (product information); The Dow Chemical Company; Freeport, Texas, 2006.
21. Wunderlich, B. Macromolecular Physics; Academic Press: New York, 1980; Vol. 3, p 42.
22. Geil, P. H. Polymer Single Crystals; Wiley-Interscience: New York, 1963; Chapter 6.
23. Mathot, V. B. F. In Calorimetry and Thermal Analysis of Polymers; Mathot, V. B. F., Ed.; Hanser: New York, 1994; Chapter 9, p 231.
24. Boyer, R. F. J Macromol Sci Phys 1973, 8, 521.
25. Boyd, R. H. Polymer 1985, 26, 1123.
26. Popli, R.; Glotin, M.; Mandelkern, L.; Benson, R. S. J Polym Sci Polym Phys Ed 1984, 22, 407.
27. Nitta, K.-H.; Tanaka, A. Polymer 2001, 42, 1219.
28. Christenson, E. M.; Anderson, J. M.; Hiltner, A.; Baer, E. Polymer 2005, 46, 11744.
29. Wang, H.; Taha, A.; Chum, S. P.; Hiltner, A.; Baer, E. ANTEC Soc Plast Eng 2007, 65, 1186.
30. Ball, R. C.; Doi, M.; Edwards, S. F.; Warner, M. Polymer 1981, 22, 1010.
31. Edwards, S. F.; Vilgis, T. Polymer 1986, 27, 483.
32. Brereton, M. G.; Klein, P. G. Polymer 1988, 29, 970.